Complex-type *N*-glycan recognition by potent broadly neutralizing HIV antibodies

Hugo Mouquet[a,1,2], Louise Scharf[b,1,2], Zelda Euler[c], Yan Liu[d], Caroline Eden[a], Johannes F. Scheid[a,e], Ariel Halper-Stromberg[a], Priyanthi N. P. Gnanapragasam[b], Daniel I. R. Spencer[f], Michael S. Seaman[g], Hanneke Schuitemaker[c], Ten Feizi[d], Michel C. Nussenzweig[a,2,3], and Pamela J. Bjorkman[b,2,3]

[a]Laboratory of Molecular Immunology, The Rockefeller University, New York, NY 10021; [b]Division of Biology, California Institute of Technology, Pasadena, CA 91125; [c]Department of Experimental Immunology, Academic Medical Center, 1105 AZ Amsterdam, The Netherlands; [d]Glycosciences Laboratory, Department of Medicine, Imperial College London, London, W12 0NN, United Kingdom; [e]Charité Universitätsmedizin, 10117 Berlin, Germany; [f]Ludger Ltd., Culham Science Centre, Abingdon, Oxfordshire OX14 3EB, United Kingdom; and [g]Beth Israel Deaconess Medical Center, Boston, MA 02215

Contributed by Pamela J. Bjorkman, October 4, 2012 (sent for review September 15, 2012)

Broadly neutralizing HIV antibodies (bNAbs) can recognize carbohydrate-dependent epitopes on gp120. In contrast to previously characterized glycan-dependent bNAbs that recognize high-mannose *N*-glycans, PGT121 binds complex-type *N*-glycans in glycan microarrays. We isolated the B-cell clone encoding PGT121, which segregates into PGT121-like and 10-1074–like groups distinguished by sequence, binding affinity, carbohydrate recognition, and neutralizing activity. Group 10-1074 exhibits remarkable potency and breadth but no detectable binding to protein-free glycans. Crystal structures of unliganded PGT121, 10-1074, and their likely germ-line precursor reveal that differential carbohydrate recognition maps to a cleft between complementarity determining region (CDR)H2 and CDRH3. This cleft was occupied by a complex-type *N*-glycan in a "liganded" PGT121 structure. Swapping glycan contact residues between PGT121 and 10-1074 confirmed their importance for neutralization. Although PGT121 binds complex-type *N*-glycans, PGT121 recognized high-mannose-only HIV envelopes in isolation and on virions. As HIV envelopes exhibit varying proportions of high-mannose- and complex-type *N*-glycans, these results suggest promiscuous carbohydrate interactions, an advantageous adaptation ensuring neutralization of all viruses within a given strain.

Antibodies are essential for the success of most vaccines (1), and antibodies against HIV appear to be the only correlate of protection in the recent RV144 anti-HIV vaccine trial (2). Some HIV-1–infected patients develop broadly neutralizing serologic activity against the gp160 viral spike 2–4 y after infection (3–10), but these antibodies do not generally protect infected humans because autologous viruses escape through mutation (11–13). Nevertheless, broadly neutralizing activity puts selective pressure on the virus (13) and passive transfer of broadly neutralizing antibodies (bNAbs) to macaques protects against simian/human immunodeficiency virus (SHIV) infection (14–24). It has therefore been proposed that vaccines that elicit such antibodies may be protective against HIV infection in humans (10, 25–28).

The development of single-cell antibody cloning techniques revealed that bNAbs target several different epitopes on the HIV-1 gp160 spike (29–35). The most potent HIV-1 bNAbs recognize the CD4 binding site (CD4bs) (31, 34, 36) and carbohydrate-dependent epitopes associated with the variable loops (32, 33, 37, 38), including the V1/V2 (antibodies PG9/PG16) (33) and V3 loops (PGTs) (32). Less is known about carbohydrate-dependent epitopes because the antibodies studied to date are either unique examples or members of small clonal families.

To better understand the neutralizing antibody response to HIV-1 and the epitope targeted by PGT antibodies, we isolated members of a large clonal family dominating the gp160-specific IgG memory response from the clade A-infected patient who produced PGT121. We report that PGT121 antibodies segregate into two groups, a PGT121-like and a 10-1074–like group, according to sequence, binding affinity, neutralizing activity, and recognition of carbohydrates and the V3 loop. The 10-1074 antibody and related family members exhibit unusual potent neutralization, including broad reactivity against newly transmitted viruses. Unlike previously characterized carbohydrate-dependent bNAbs, PGT121 binds to complex-type, rather than high-mannose, *N*-glycans in glycan microarray experiments. Crystal structures of PGT121 and 10-1074 compared with structures of their germ-line precursor and a structure of PGT121 bound to a complex-type *N*-glycan rationalize their distinct properties.

Results

Predominance and Diversity of PGT121 Clonotype. We recently isolated gp140-specific IgG memory B cells from a clade A-infected African donor [described as pt10 (39) or patient 17 (32)], using YU-2 gp140 trimers as "bait." Eighty-seven matching Ig heavy (IgH)- and light (IgL)-chain genes corresponding to 23 unique clonal families were identified. The IgH anti-gp140 repertoire was dominated by one clonal family representing ~28% of all expanded B-cell clones (Fig. 1*A*). This B-cell family corresponds to the same clone as PGT121–123 (32) and contained 38 members, 29 of which were unique variants at the nucleotide level (Fig. 1*A* and *SI Appendix*, Table S1). On the basis of their IgH nucleotide sequence, the PGT121 family divides into two groups: a PGT121-like group containing PGT121–123 and nine closely related variants and a second group, 10-1074–like, containing 20 members (Fig. 1*A*). Although our traditional primers (40, 41) did not amplify the IgL genes expressed by the PGT121 B-cell clone due to the nucleotide deletions in the region encoding framework region 1, 24 of 38 Igλ genes were obtained using new Igλ-specific primers designed to amplify heavily somatically mutated genes (*SI Appendix*, Table S1). Consistent with the high levels of hypermutation in the IgH genes (18.2% of the VH gene on average), the amplified Igλ genes were highly mutated (18.2% of the Vλ gene on average) and carried nucleotide deletions in framework region 1 (FWR1) (12–21 nt) and a 9-nt insertion in framework region 3 (FWR3) (*SI Appendix*, Fig. S1*B* and Table S1).

Author contributions: H.M and M.C.N conceived the project; H.M., L.S., Z.E., Y.L., H.S., T.F., M.C.N., and P.J.B. designed research; H.M., L.S., Z.E., Y.L., H.S., T.F., M.C.N., and P.J.B. performed research; H.M. produced the antibodies and the HIV Env proteins; H.M. performed and analyzed antibody-binding experiments; L.S. determined and interpreted crystal structures; C.E., J.F.S., and A.H.-S. contributed new reagents/analytic tools; Z.E. and H.S. performed and analyzed PBMC-based neutralization assays; Y.L. performed carbohydrate microarray analyses; P.N.P.G. performed and analyzed neutralization assays using viral strains produced in GnTI $^{-/-}$ cells; D.I.R.S. isolated and characterized the NA2 glycan; M.S.S. performed and analyzed TZM-bl neutralization assays; and H.M., L.S., Y.L., T.F., M.C.N., and P.J.B. wrote the paper.

Conflict of interest statement: M.C.N., H.M., P.J.B. and L.S. have a pending patent application for the new PGT121 antibody variants described in the present study with the United States Patent and Trademark Office.

Freely available online through the PNAS open access option.

Data deposition: The atomic coordinates and structure factors have been deposited in the Protein Data Bank, www.pdb.org [PDB ID codes 4FQ1 (unliganded PGT121 Fab), 4FQC ("liganded" PGT121 Fab), 4FQ2 (10-1074 Fab), and 4FQQ (GL Fab)].

[1]H.M. and L.S. contributed equally to this work.

[2]To whom correspondence may be addressed. E-mail: hmouquet@rockefeller.edu, lscharf@caltech.edu, nussen@rockefeller.edu, or bjorkman@caltech.edu.

[3]M.C.N. and P.J.B. contributed equally to this work.

See Author Summary on page 19059 (volume 109, number 47).

This article contains supporting information online at www.pnas.org/lookup/suppl/doi:10.1073/pnas.1217207109/-/DCSupplemental.

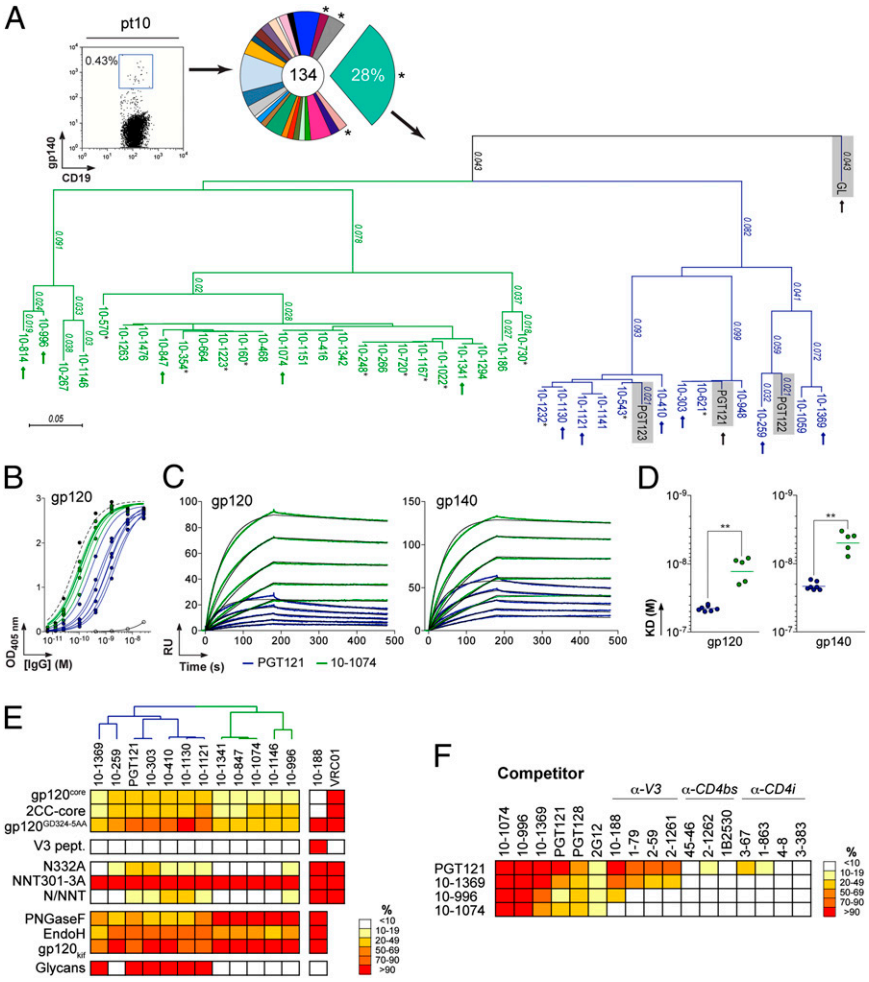

Fig. 1. PGT121 and 10-1074 clonal variants. (*A*) (*Left*) Cytogram showing staining of pt10 PBMCs. (*Center*) Pie chart showing the expansion of gp140-specific IgG memory B cells. *, no matching IgL was initially found. (*Right*) Dendrogram showing the relationship between PGT121-like (blue) and 10-1074–like (green) IgH protein sequences with PGT121, PGT122, PGT123, and GL sequences (gray shading) included for comparison. Arrows indicate clones that were produced as IgGs. Underlined clones were not identical at the nucleotide level. *, no matching IgL could be amplified due to limited cDNA material. (*B*) ELISA comparisons of binding. Curves show the binding of 10-1074–like (green) and PGT121-like (blue) antibodies to YU-2 gp120. Black dashed and solid lines show positive (10-188) and negative (mG053) controls, respectively. (*C*) SPR sensorgrams showing the binding of 10-1074 (green) and PGT121 (blue) to YU-2 gp120 or gp140. Fits to a 1:1 binding model are shown in black. RU, response units. (*D*) Apparent K_D values for the binding of 10-1074–like (green dots) and PGT121-like (blue dots) antibodies to gp120 and gp140. $^{**}P < 0.005$. (*E*) Heat map (expressed as percentage of binding to unmodified gp120) summarizing the binding of PGT121-like and 10-1074–like antibodies [listed with a dendrogram showing their relationships (*A*)] to diverse antigens (*SI Appendix*, Figs. S3–S8). Darker colors, stronger binding; white, no observed binding. Anti-gp120^{V3} (10-188) and anti-CD4bs (VRC01) antibodies are controls. For V3 loop peptide-binding assays (V3 pept.) and glycan arrays, red indicates binding and white indicates no binding. (*F*) Competition ELISAs. Heat map showing the relative binding to gp120 of selected PGT121-like and 10-1074–like antibodies in the presence of potential competitor antibodies (*SI Appendix*, Fig. S8). Results are expressed as percentage of binding in presence of 100 μg/mL of competitor compared with binding in the absence of competitor. Darker colors indicate stronger inhibition; white indicates no competition.

We expressed 11 new unique variants (Fig. 1*A* and *SI Appendix*, Table S1) and demonstrated binding to YU-2 gp120 and gp140 by ELISA and surface plasmon resonance (SPR) (Fig. 1 *B*–*D*). Unless otherwise noted, the gp120 and gp140 proteins for these and other experiments were expressed in mammalian cells that can attach either a complex-type or a high-mannose *N*-glycan to a potential *N*-glycosylation site (PNGS). The level of reactivity with gp120 differed between antibodies belonging to the PGT121 and 10-1074 groups, the latter exhibiting higher apparent affinities (Fig. 1 *C* and *D* and *SI Appendix*, Fig. S2*A*) mainly due to slower dissociation from gp120/gp140 for the 10-1074–related antibodies (*SI Appendix*, Fig. S2*B*).

PGT121 and 10-1074 Epitopes. Asn332$_{gp120}$ in the vicinity of the V3 loop stem was reported as critical for binding and viral neutralization by PGT121 (32); thus we examined the role of V3 in antigen recognition by PGT121-like and 10-1074–like antibodies. ELISAs were performed using HxBc2 gp120 "core" proteins that lack V1–V3 loops (gp120^{core}) or retain a portion of V3 (2CC-core) and using a YU-2 gp120 mutant protein carrying a double-alanine substitution in the V3 stem (gp120$^{GD324-5AA}$). The tested antibodies showed decreased reactivity against variants lacking the V3 loop and gp120$^{GD324-5AA}$ compared with intact YU-2 gp120, with the binding of 10-1074–group antibodies being the most affected (Fig. 1*E* and *SI Appendix*, Fig. S3 *A* and *B*). These results suggest that recognition by both antibody groups involves protein determinants in the vicinity of the V3 loop. None of the antibodies bound to overlapping peptides spanning V3, suggesting the targeted epitopes are discontinuous and/or require a particular conformation not achieved by isolated peptides (Fig. 1*E* and *SI Appendix*, Fig. S3*C*).

Asn332$_{gp120}$ [Asn337$_{gp120}$ in earlier numbering (42)] is the N-terminal residue of a PNGS defined as the sequence Asn–X–Ser/Thr. To determine whether Asn332$_{gp120}$ and/or its *N*-linked glycan are required for gp120 reactivity of the new PGT121-group and 10-1074–group antibodies, we tested their binding to YU-2 gp120^{N332A} by ELISA. The N332A substitution diminished the binding of PGT121 (32) and all of the new antibody variants, whereas their reactivity against a mutant gp120 lacking a nearby glycosylation site (gp120$^{NNT301-3AAA}$ mutant) was unchanged (Fig. 1*E* and *SI Appendix*, Fig. S4*A*). To determine whether a PNGS in addition to the Asn332$_{gp120}$ PNGS affects recognition by the new antibodies, we constructed a series of 11 double-glycan mutants in which the N332A mutation in YU-2 gp120 was combined with mutation of PNGSs located between Asn262$_{gp120}$ and Asn406$_{gp120}$ (*SI Appendix*, Fig. S5). All of the PGT121-like and 10-1074–like antibodies bound to each of the double-glycan mutants with comparable affinity to that for gp120^{N332A} (*SI Appendix*, Fig. S5), and thus we did not find another PNGS that further affected binding by PGT121-group or 10-1074–group antibodies.

To compare overall glycan recognition by the PGT121-like and 10-1074–like antibodies, we examined their binding to YU-2 gp120 treated with PNGase F, which cleaves both complex-type and high-mannose *N*-glycans. Because gp120 cannot be fully deglycosylated enzymatically unless it is denaturated, PNGase F treatment resulted in partial deglycosylation of natively folded gp120 (*SI Appendix*, Fig. S4*B*). Nevertheless, the reactivities of the two groups of antibodies differed in that partial deglycosylation of gp120 by PNGase F decreased the binding activity of all PGT121-like antibodies but none of the 10-1074–like antibodies (Fig. 1*E* and *SI Appendix*, Fig. S4*C*). Similar experiments conducted with YU-2 gp120 treated with Endo

H, which cleaves high-mannose, but not complex-type, *N*-glycans, affected binding of 10-1074–like antibodies more than that of PGT121-like antibodies (Fig. 1*E* and *SI Appendix*, Fig. S4*D*).

An *N*-glycan microarray revealed that six of seven tested PGT121-like antibodies showed detectable binding to complex-type mono- or biantennary *N*-glycans terminating with galactose or α2–6-linked sialic acid but no detectable binding to high-mannose–type glycans, corroborating and extending previous reports of no binding of PGT121-123 to high-mannose *N*-glycans and no competition by Man_4 and Man_9 dendrons for gp120 binding (32) (Fig. 1*E* and *SI Appendix*, Fig. S6). In contrast, there was no detectable binding to protein-free glycans by 10-1074–like antibodies (Fig. 1*E* and *SI Appendix*, Fig. S6). Although PGT121-like antibodies bound to protein-free complex-type, but not high-mannose, *N*-glycans, PGT121-like antibodies retained binding to YU-2 gp120 produced in cells treated with kifunensine ($gp120_{kif}$), a mannosidase inhibitor that results in exclusive attachment of high-mannose glycans to PNGSs (43) (Fig. 1*E* and *SI Appendix*, Fig. S7*B*). Most of the PGT121-like antibodies exhibited a small, but reproducible, decrease in binding to $gp120_{kif}$. By contrast, 10-1074–like antibodies retained full binding to $gp120_{kif}$ (Fig. 1*E* and *SI Appendix*, Fig. S7*B*). These results are consistent with the hypothesis that high-mannose, as well as complex-type, *N*-glycans can be involved in the epitope of PGT121-like antibodies.

Epitope-mapping experiments were performed with two representative members of each group (PGT121 and 10-1369 for the PGT121-like group and 10-1074 and 10-996 for the 10-1074–like group) by competition ELISA. All four antibodies showed cross-competition, but PGT121 more modestly inhibited the binding of 10-996 and 10-1074 to gp120 than vice versa (Fig. 1*F* and *SI Appendix*, Fig. S8). To further map the targeted epitopes, we used anti-gp120 antibodies that recognize the crown of the V3 loop (SI Appendix, Fig. S3*C*) (39, 44), the CD4bs (31, 44), the coreceptor binding site [CD4-induced (CD4i)] (44), a constellation of high-mannose *N*-glycans (2G12) (45–48), or the V3 loop and *N*-linked glycans at positions 301 and 332 (PGT128) (32, 37). Anti-V3 crown antibodies inhibited the binding of PGT121 and 10-1369 but did not interfere with the binding of 10-996 and 10-1074 (Fig. 1*F* and *SI Appendix*, Fig. S8). PGT128, and to a lesser extent 2G12, but not the CD4bs and CD4i antibodies, diminished the binding of all four antibodies to gp120 (Fig. 1*F* and *SI Appendix*, Fig. S8).

Taken together, these data suggest that PGT121 clonal members recognize a site involving a protein determinant in the vicinity of the V3 loop and the $Asn332_{gp120}$-associated glycan (*SI Appendix*, *Discussion*). However, the clone segregates into two families, the PGT121-like and 10-1074–like groups, which differ in their affinities for gp120 and in the role of glycans in epitope formation.

Broad and Potent HIV Neutralization. To evaluate the neutralizing activity of the new PGT121 variants, we measured their ability to inhibit HIV infection of TZM-bl cells (49), using 10 viral strains including R1166.c1, which lacks the PNGS at gp120 position 332. All PGT121 variants, including the 10-1074–like antibodies, neutralized nine pseudoviruses and none neutralized the R1166.c1 control (Fig. 2*A* and *SI Appendix*, Table S2). Neutralizing activity correlated with affinity for the HIV spike, with the 10-1074 group showing slightly greater potencies than the PGT121 group (Fig. 2*B* and *SI Appendix*, Fig. S2*C*). A representative germ-line (GL) version of the PGT121/10-1074 antibody clonotype (*SI Appendix*, *Methods*) failed to bind gp120/gp140 or neutralize any viruses in the panel, implying that somatic mutation is required for binding and neutralization (*SI Appendix*, Fig. S9). Pairing GL light chains with mutated 10-1074– or 10-996–group heavy chains failed to rescue binding or neutralization, suggesting that both mutated chains contribute to proper assembly of the antibody paratope (*SI Appendix*, Fig. S9).

We next compared the neutralization activities of PGT121 and two 10-1074–like antibodies (10-996 and 10-1074) against an extended panel of 119 difficult-to-neutralize pseudoviruses (classified as tier-2 and tier-3) (31) (*SI Appendix*, Tables S3 and S4). The 10-996 and 10-1074 antibodies showed neutralization potencies and breadth similar to those of PGT121 (Fig. 2*C* and *SI Appendix*, Fig. S10 and Tables S3 and S4). As anticipated, most viruses bearing

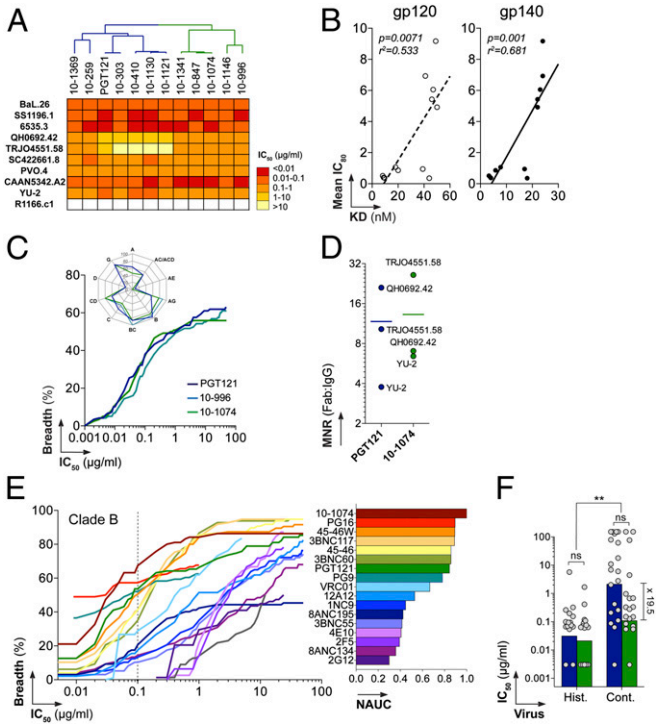

Fig. 2. Neutralization activity of PGT121-like and 10-1074–like variants. (*A*) Heat map comparing the neutralization potencies of PGT121-like and 10-1074–like antibodies (listed at the top with a dendrogram showing relationships; Fig. 1*A*) in the TZM-bl assay. Darker colors, more potent neutralization; white, no neutralization. (*B*) Correlation between the mean IC_{80} against nine viruses (*y* axis) and apparent K_D values for binding to gp120 and gp140 (*x* axis). (*C*) Graph comparing the neutralization breadth and potencies of PGT121, 10-996, and 10-1074 antibodies in the TZM-bl assay against an extended panel of 119 viruses. The *y* axis shows the cumulative frequency of IC_{50} values up to the concentration shown on the *x* axis. The spider graph (upper left) shows the frequency distribution of neutralized viruses according to HIV-1 clades. (*D*) Dot plot showing molar neutralization ratios (MNRs) (ratio of the Fab and IgG IC_{50} concentrations). Horizontal bars represent the mean IC_{50}s for all viruses. (*E*) Coverage graph (as in *C*) comparing the neutralization breadth and potencies of selected bNAbs against a panel of 95 clade B viruses as evaluated by the PBMC-based neutralization assay. (*Right*) Bar graph showing values for the normalized area under the curve (NAUC) for the IgGs shown in the coverage graph. (*F*) Bar graph comparing the neutralization potencies of PGT121 (blue) and 10-1074 (green) against viruses isolated from historical (Hist.) and contemporary (Cont.) seroconverters. ns, nonsignificant; $^{**}P < 0.005$. Fold difference between median IC_{50}s for the neutralization of contemporary viruses by PGT121 and 10-1074 is indicated.

amino acid changes at gp120 positions 332 and/or 334 (spanning the Asn332–X–Ser334/Thr334 PNGS) were resistant to neutralization (83.8% were resistant to PGT121, and 100% were resistant to 10-1074 and 10-996). Mutation at this PNGS accounted for the majority of viruses resistant to neutralization (68.5% for 10-996, 72.5% for 10-1074, and 60.8% for PGT121) (*SI Appendix*, Table S5). Comparable neutralization activities were observed for the IgG and fragment antigen binding (Fab) forms of PGT121 and 10-1074, suggesting that bivalency is not critical for their activity (Fig. 2*D*).

To evaluate the potential role of complex-type *N*-glycans on the HIV envelope in neutralization by PGT121 and 10-1074, we produced high-mannose-only virions in two different ways: by assembling pseudoviruses in cells treated with kifunensine, which results in $Man_9GlcNAc_2$ *N*-linked glycans, or by assembly in HEK 293S GnTI $^{-/-}$ cells, which results in $Man_5GlcNAc_2$ *N*-linked glycans (50). We found that PGT121 neutralized two of three kifunensine-derived PGT121-sensitive/10-1074–resistant strains equivalently to their counterparts produced in wild-type cells (*SI Appendix*, Fig. S7*C*). Two PGT121-sensitive/10-1074–sensitive viral strains produced in GnTI $^{-/-}$ cells were equally as sensitive to PGT121 and

10-1074 as their counterparts produced in wild-type cells. Consistent with previous reports that complex-type *N*-glycans partially protect the CD4 binding site from antibody binding (50), the viruses produced in GnTI $^{-/-}$ cells were more sensitive to CD4-binding–site antibodies (NIH45-46^{G54W} and 3BNC60) (*SI Appendix*, Fig. S7*D*).

Newly Transmitted HIV-1. We next examined the activity of PGT121 and 10-1074 against transmitted founder viruses by evaluating neutralization in a peripheral blood mononuclear cell (PBMC)-based assay, using 95 clade B viruses isolated from a cohort of individuals who seroconverted between 1985 and 1989 (historical seroconverters, $n = 14$) or between 2003 and 2006 (contemporary seroconverters, $n = 25$) (51, 52). We compared PGT121 and 10-1074 with anti-CD4bs bNAbs (31) and other bNAbs including VRC01, PG9/PG16, b12, 2G12, 4E10, and 2F5 (51, 52). Clustering analyses of neutralization activity showed segregation into two groups; the PGT121/10-1074 group contained the most active HIV neutralizers including the anti-CD4bs and PG9 antibodies (*SI Appendix*, Fig. S11*A* and Table S6). Remarkably, 10-1074 showed exceptional neutralization potency on this clade B virus panel, exhibiting the greatest breadth at 0.1 μg/mL (67% of the 95 clade B viruses) of all bNAbs tested (Fig. 2*E* and *SI Appendix*, Fig. S11*B* and Table S6). Although 10-1074 showed higher potency on contemporary clade B viruses than PGT121 (~20-fold difference), both antibodies were more effective against historical than contemporary viruses (Fig. 2*F* and *SI Appendix*, Fig. S11*C*).

Crystal Structures of PGT121, 10-1074, and GL. To investigate the structural determinants of the differences between PGT121-like and 10-1074-like antibodies, we solved crystal structures of the Fab fragments of PGT121, 10-1074, and a representative GL precursor at 3.0 Å, 1.9 Å, and 2.4 Å resolution, respectively (*SI Appendix*, Table S7). Superimposition of the heavy- and light-chain variable domains (V_H and V_L) among the three Fabs showed conservation of the backbone structure, with differences limited to small displacements of the complementarity determining region (CDR) H3 and CDRL3 loops of the affinity-matured Fabs relative to GL (Fig. 3*A* and *SI Appendix*, Fig. S12 and Table S8).

An unusual feature shared by the antibodies is their long (25 residues) CDRH3 loop, which forms a two-stranded antiparallel β-sheet extending the V_H domain F and G strands (Fig. 3*B*). In each Fab, the tip of the extended CDRH3 loop primarily contains nonpolar residues (Fig. 3*B*). A similar structural feature was observed for the CDRH3 of PGT145, a carbohydrate-sensitive antibody whose epitope involves the gp120 V1V2 loop (38). However, the extended two-stranded β-sheet of PGT145's CDRH3 contains mostly negatively charged residues, including two sulfated tyrosines at the tip. Aligning V_H-V_L of PGT121 and PGT145 (*SI Appendix*, Table S8) shows that CDRH3$_{PGT145}$ extends past CDRH3$_{PGT121}$ and that its tip and V_H domain are aligned, whereas the CDRH3s of PGT121, 10-1074, and GL tilt toward V_L (*SI Appendix*, Fig. S13*A*). The tilting of CDRH3$_{PGT121}$/CDRH3$_{10\text{-}1074}$/CDRH3$_{GL}$ toward V_L opens a cleft between CDRH2 and CDRH3 (Fig. 3 *C* and *D*), a feature not shared by related antibodies (*SI Appendix*, Fig. S13).

PGT121 and 10-1074 are highly divergent with respect to GL and each other (of 132 residues, PGT121$_{VH}$ differs from 10-1074$_{VH}$ and GL$_{VH}$ by 36 and 45 residues, respectively, and 10-1074$_{VH}$ and GL$_{VH}$ differ by 29) (Fig. 3 and *SI Appendix*, Fig. S14). The majority of the PGT121/10-1074 differences are located in the CDR$_{VH}$ loops and CDRL3. Interestingly, six substitutions in CDRH3 (residues 100d, 100f, 100h, 100j, 100l, and 100n) alternate such that every second residue is substituted, causing resurfacing of the cleft between CDRH2 and CDRH3 that results from CDRH3 tilting toward V_L (Fig. 3 *C* and *D*). This region likely contributes to the different fine specificities of PGT121 and 10-1074. Five other solvent-exposed substitutions in heavy-chain framework region 3 (FWR3$_{HC}$) (residues 64, 78, and 80–82; strands D and E) are potential antigen contact sites (Fig. 3 *C* and *D* and *SI Appendix*, Fig. S14) given that framework regions in HIV antibodies can contact gp120 (31, 36, 53). Other differences that may contribute to fine specificity differences include a negative patch on PGT121 in the vicinity of Asp56$_{HC}$ not present in 10-1074 or GL (Ser56$_{HC}$ in 10-1074 and GL) and positive patches on the CDRL1 and CDRL3 surface not found on the analogous surface of GL (*SI Appendix*, Fig. S15).

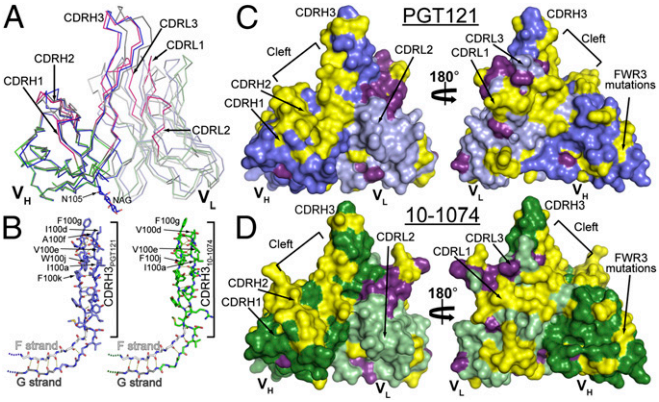

Fig. 3. Comparison of PGT121, 10-1074, and GL Fab structures. (*A*) Cα alignment of variable domains of PGT121 (VH$_{PGT121}$, blue; VL$_{PGT121}$, light blue), 10-1074 (VH$_{10\text{-}1074}$, green; VL$_{10\text{-}1074}$, light green) and GL (VH$_{GL}$, dark gray; VL$_{GL}$, light gray) (CDRs for 10-1074 are magenta). An *N*-acetylglucosamine attached to PGT121 Asn105$_{HC}$ is depicted as sticks. (*B*) CDRH3 loops of PGT121 and 10-1074. Extensions of the V_H domain F (white) and G (grey) strands (only main chain atoms shown) form CDRH3, a two-stranded β-sheet in PGT121 (blue), 10-1074 (green), and GL (main and side chain atoms shown; main chain hydrogen bonds are yellow dashes). (*C* and *D*) Surface representation of PGT121 (*C*) and 10-1074 (*D*) variable domains showing differences (yellow) and somatic mutations in common (purple). PGT121 HC, blue; PGT121 LC, light blue; 10-1074 HC, green; 10-1074 LC, light green.

Somatic mutations common to PGT121 and 10-1074 may be involved in shared features of their epitopes. The heavy chains of PGT121 and 10-1074 share only three common mutations (of 36 PGT121–GL and 29 10-1074–GL differences) (Fig. 3 *C* and *D*). In contrast, PGT121 and 10-1074 share 18 common light-chain mutations (of 37 PGT121–GL and 36 10-1074–GL differences), including an insertion in light-chain FWR3 that causes bulging of the loop connecting strands D and E (Fig. 3 *C* and *D* and *SI Appendix*, Fig. S12), and the substitution of Asp50$_{LC}$-Asp51$_{LC}$ in CDRL2$_{GL}$ to Asn50$_{LC}$-Asn51$_{LC}$ in both PGT121 and 10-1074, resulting in a less negatively charged surface (*SI Appendix*, Fig. S15). The large number of common substitutions introduced into light chain (LC)$_{PGT121}$ and LC$_{10\text{-}1074}$ (~50% of LC substitutions) points to CDRL1, CDRL2, and FWR2$_{LC}$ as potential contact regions for epitopes shared by PGT121 and 10-1074.

We next made comparisons with the structure of PGT128, which recognizes Asn332$_{gp120}$- and Asn301$_{gp120}$-linked glycans and V3 and was solved as a complex with an outer-domain/mini-V3 loop gp120 expressed in cells that cannot produce complex-type *N*-glycan–modified proteins (37). Unlike the CDRH3 loops of PGT121 and 10-1074, PGT128$_{CDRH3}$ is not tilted toward PGT128$_{VL}$, and CDRH3$_{PGT128}$ does not include a two-stranded β-sheet (*SI Appendix*, Fig. S13). In addition, CDRH3$_{PGT128}$ (18 residues) is shorter than the CDRH3s of PGT121 and 10-1074 (24 residues), whereas CDRH2$_{PGT128}$ contains a 6-residue insertion not found in PGT121 or 10-1074. Due to these differences, CDRH2 is the most prominent feature in PGT128, whereas CDRH3 is most prominent in PGT121 and 10-1074 (*SI Appendix*, Fig. S13). CDRH2$_{PGT128}$ and CDRL3$_{PGT128}$ together recognize Man$_{8/9}$ attached to Asn332$_{gp120}$, and CDRH3$_{PGT128}$ contacts the V3 loop base. This mode of gp120 recognition is not possible for PGT121 and 10-1074 because the structural characteristics of their CDRH2 and CDRH3 loops differ significantly from those of PGT128 (*SI Appendix*, Fig. S13), consistent with the ability of PGT128 (37), but not PGT121 and 10-1074 (*SI Appendix*, Fig. S6), to recognize protein-free high-mannose glycans.

Crystal Structure of PGT121–Glycan Complex. A 2.4-Å resolution structure of PGT121 associated with a complex-type sialylated

biantennary glycan was solved (Fig. 4 and *SI Appendix*, Table S7) using crystals obtained under conditions including NA2, a complex-type asialyl biantennary glycan (*SI Appendix*, Fig. S6). Surprisingly, the glycan bound to PGT121 in our crystal structure was not NA2, but rather a complex-type *N*-glycan from a neighboring PGT121 Fab in the crystal lattice: specifically the *N*-glycan attached to Asn105$_{HC}$ (*SI Appendix*, Fig. S16*A*). The glycan identity is evident because there was electron density for the glycosidic linkage to Asn105$_{HC}$ and for a terminal sialic acid on the Manα1–3Man antenna (the galactose and sialic acid moieties of the Manα1–6Man antenna were unresolved) (*SI Appendix*, Fig. S17*A*). The composition of the bound glycan corresponds to a portion of the α2–6-sialylated A2(2–6) glycan that was bound by PGT121 in microarray experiments (*SI Appendix*, Fig. S6) and to the expected sialyl linkage on complex-type *N*-glycans attached to PNGS on proteins expressed in HEK293T cells (54). Although the V_H-V_L domains of this structure ("liganded" PGT121) superimpose with no significant differences onto the V_H-V_L domains of the PGT121 structure with no bound *N*-glycan ("unliganded" PGT121) (*SI Appendix*, Fig. S16*B* and Table S8), the elbow bend angle (angle between the V_H–V_L and C_H1–C_L pseudodyads) differs between the structures (*SI Appendix*, Fig. S16). This difference likely reflects flexibility that allows the Fab to adopt variable elbow bend angles depending upon crystal lattice forces.

Given that we observed binding of complex-type *N*-glycan in one crystal structure (the liganded PGT121 structure) but not in another structure (the unliganded PGT121 structure), we estimate that the affinity of PGT121 for complex-type *N*-glycan not attached to gp120 is in the range of the concentration of PGT121 in crystals (~10 mM). If we assume that the K_D for binding isolated glycan is in the range of 1–10 mM, comparable to the 1.6-mM K_D derived for PG9 binding to $Man_5GlcNAc_2$-Asn (38), then the K_D for PGT121 binding of isolated glycan represents only a minor contribution to the affinity of PGT121 for gp120, which is in the nanomolar range (*SI Appendix*, Fig. S2*A*).

The glycan in the liganded PGT121 structure interacts exclusively with the V_H domain and makes extensive contacts with residues in all three CDRs (buried surface area on PGT121$_{HC}$ = 600 Å^2). Contacts include 10 direct and 18 water-mediated hydrogen bonds (*SI Appendix*, Table S9) with 9 aa anchoring the glycan between the *N*-acetylglucosamine moiety linked to the branch-point mannose and the terminal sialic acid on the 1–3 antenna (Fig. 4 and *SI Appendix*, Fig. S17*B*). Several contacts with PGT121 are made by this sialic acid, including three direct hydrogen bonds with PGT121 residues Asp31$_{HC}$ and His97$_{HC}$ in addition to water-mediated hydrogen bonds with Asp31$_{HC}$. The sialic acid also contributes to a water-mediated intraglycan hydrogen bond network (Fig. 4). The direct contacts with sialic acid may explain the stronger binding of PGT121 to the sialylated A2(2–6) glycan than to the asialylated NA2 glycan in our glycan microarray analysis (*SI Appendix*, Fig. S6). Extensive water-mediated protein contacts established by the *N*-acetylglucosamine and galactose moieties of the 1–3 antenna could explain the binding observed for asialylated mono- and biantennary glycans to PGT121 (*SI Appendix*, Fig. S6).

Six of the residues contributing direct or likely amino acid side-chain contacts to the glycan (Ser32$_{HC\text{-}CDRH1}$, Lys53$_{HC\text{-}CDRH2}$, Ser54$_{HC\text{-}CDRH2}$, Asn58$_{HC\text{-}CDRH2}$, His97$_{HC\text{-}CDRH3}$, and Thr100l$_{HC\text{-}CDRH3}$) differ from those on 10-1074 (Tyr32$_{HC\text{-}CDRH1}$, Asp53$_{HC\text{-}CDRH2}$, Arg54$_{HC\text{-}CDRH2}$, Thr58$_{HC\text{-}CDRH2}$, Arg97$_{HC\text{-}CDRH3}$, and Tyr100l$_{HC\text{-}CDRH3}$) and are highly conserved among PGT121-like, but not 10-1074–like, antibodies (Fig. 4*D*). The 10-1074 residues lack the corresponding functional groups to make the observed glycan contacts or have bulky side chains that would cause steric clashes (*SI Appendix*, Fig. S14). Four of these residues also differ from those on the GL (Tyr32$_{HC\text{-}CDRH1}$, Tyr53$_{HC\text{-}CDRH2}$, Gln97$_{HC\text{-}CDRH3}$, and Tyr100l$_{HC\text{-}CDRH3}$), suggesting that the lack of binding of 10-1074–like antibodies and GL to protein-free complex-type glycans in our glycan microarrays results from missing hydrogen bonds and/or steric clashes (e.g., His97$_{PGT121}$ vs. Arg97$_{10\text{-}1074}$ and/or Thr100l$_{PGT121}$ vs. Tyr100l$_{10\text{-}1074}$). As the majority of sequence differences between PGT121 and 10-1074 cluster in the CDRH loops (Fig. 3 *C* and *D*), specifically to the surface of the cleft between CDRH2 and CDRH3 where we observe the bound complex-type *N*-glycan (Fig. 4), differential recognition of complex-type glycans on gp120 may account for some or all of the differences in their fine specificity observed in our functional experiments (Figs. 1, 2, and 4 and *SI Appendix*, Figs. S1–S8).

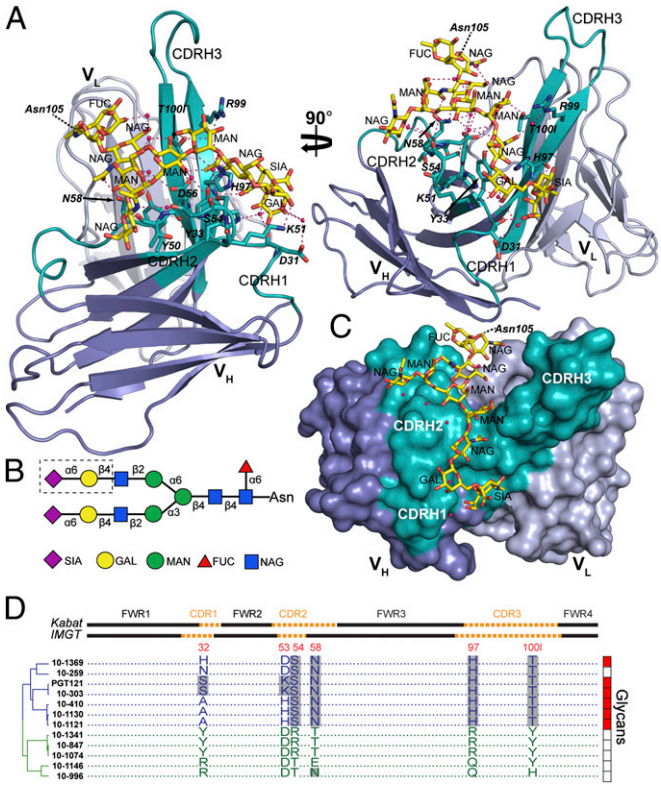

Fig. 4. Crystal structure of a liganded PGT121. (*A*) Ribbon diagram of the PGT121 variable domains bound to a complex-type *N*-glycan (yellow sticks) attached to Asn105$_{HC}$ of a neighboring Fab in the crystal. V_H is blue with CDRs highlighted in teal, V_L is light blue, side-chain and backbone atoms of contact residues are depicted as sticks, hydrogen bonds are magenta dashed lines, and water molecules are red spheres. (*B*) Schematic of the bound complex-type glycan. Glycan residues in the dashed box were disordered. Fucose (FUC), red triangles; galactose (GAL), yellow circles; mannose (MAN), green circles; *N*-acetyl glucosamine (NAG), blue squares; sialic acid (SIA), magenta diamonds. (*C*) Surface representation of PGT121 variable domains with bound glycan (sticks). Coloring is as in *A*. (*D*) Amino acid alignment comparing residues at positions 32, 53, 54, 58, 97, and 100l (residues of PGT121 making direct or likely contacts with *N*-glycan; amino acid numbering based on crystal structures) between PGT121-like (blue) and 10-1074–like (green) antibodies. Framework (FWR) and complementarity determining regions (CDR) (*Upper*), dendrogram showing relationships (*Left*), and binding to protein-free glycans as detected in glycan arrays (*Right*; red indicates binding, white indicates no binding) are indicated. Gray shading indicates amino acid identity.

Substitution of Glycan-Contacting Antibody Residues Affects Neutralization. To evaluate the contributions of complex-type *N*-glycan contacting residues identified from the liganded PGT121 structure, we generated two mutant antibodies designed to exchange the complex-type glycan-contacting residues between PGT121 and 10-1074: a 10-1074 IgG with PGT121 residues (six substitutions in IgH: Y32S, D53K, R54S, T58N, R97H, and Y100lT) and a PGT121 IgG with reciprocal substitutions. The "glycomutant" antibodies (10-1074$_{GM}$ and PGT121$_{GM}$) exhibited near–wild-type apparent affinity for YU-2 gp120/gp140 as measured by SPR (Fig. 5 *A* and *B*), demonstrating that the substitutions did not destroy binding to an envelope spike derived from a viral strain neutralized by both PGT121 and 10-1074 (Fig. 2*A*). The fact that PGT121 complex-type *N*-glycan contacting residues can be accommodated within the 10-

1074 background without destroying binding to a gp120/gp140 bound by both wild-type antibodies implies overall similarity in antigen binding despite fine specificity differences.

Unlike wild-type PGT121, PGT121$_{GM}$ showed no glycan binding in microarray experiments, confirming that 10-1074 residues at the substituted positions are not compatible with protein-free glycan binding (Fig. 5*C*) and supporting the suggestion that residues contacting the glycan in the liganded PGT121 structure are involved in recognition of complex-type glycans in the microarrays. The 10-1074$_{GM}$ protein also showed no binding to protein-free glycans (Fig. 5*C*), indicating the involvement of residues in addition to those substituted in creating the binding site for a protein-free complex-type *N*-glycan.

We next used a TZM-bl–based assay to compare neutralization of the wild-type and glycomutant antibodies. We tested 40 viral strains including strains differentially resistant to PGT121 or 10-1074 and strains sensitive to both wild-type antibodies (Fig. 5 *D* and *E* and *SI Appendix*, Table S10). Consistent with the binding of PGT121$_{GM}$ and 10-1074$_{GM}$ to purified YU-2 envelope proteins (Fig. 5*A*), both mutants neutralized the YU-2 virus (Fig. 5*D*); however, 64% of the PGT121-sensitive strains were resistant to PGT121$_{GM}$ (Fig. 5 *D* and *E* and *SI Appendix*, Table S10), suggesting that the glycan-contacting residues identified in the liganded PGT121 structure are relevant to the neutralization activity of PGT121. Conversely, 10-1074$_{GM}$ exhibited a higher average potency than wild-type 10-1074 against the 10-1074–sensitive strains (Fig. 5*E* and *SI Appendix*, Table S10), including potency increases of more than threefold against four 10-1074–sensitive strains (WITO4160.33, ZM214M.PL15, Ce1172_H1, and 3817.v2.c59). In general, the PGT121 substitutions into 10-1074 did not confer sensitivity to 10-1074$_{GM}$ upon PGT121-sensitive/10-1074–resistant strains; however, two of these strains (CNE19 and 62357_14_D3_4589) became sensitive to 10-1074$_{GM}$ (IC$_{50}$s = 0.19 μg/mL and 40.8 μg/mL, respectively) (Fig. 5*D*). Interestingly, these are the only PGT121-sensitive/10-1074–resistant strains that include an intact Asn332$_{gp120}$-linked PNGS (Fig. 5*D*). The other PGT121-sensitive/10-1074–resistant strains lack the Asn332$_{gp120}$-linked glycan and are resistant to PGT121$_{GM}$ and 10-1074$_{GM}$, implying that their sensitivity to wild-type PGT121 involves a nearby *N*-glycan and/or compensation by protein portions of the epitope (*SI Appendix*, *Discussion*). Although a dramatic gain of function was observed only for 10-1074$_{GM}$ against one strain (CNE19), this result, together with the general improvement observed for 10-1074$_{GM}$ against 10-1074–sensitive strains (Fig. 5*E*), is consistent with the interpretation that the crystallographically identified glycan-contacting residues can transfer PGT121-like recognition properties to 10-1074 in some contexts and/or affect its potency in others. In addition, the loss of neutralization activity for PGT121$_{GM}$ against PGT121-sensitive strains demonstrates that neutralization activity of PGT121 involves residues identified as contacting complex-type *N*-glycan in the liganded PGT121 structure.

Discussion

The HIV spike is covered by carbohydrates that can act as a shield to protect the virus against antibodies (13, 50). This strategy appears to be largely successful in most infected individuals, although a small number of patients develop bNAbs that bind in part to glycans (32, 33, 47). The involvement of glycan recognition in the activities of bNAbs against HIV-1 ranges from that of 2G12, which binds a constellation of high-mannose glycans with little input from specific protein binding (47), to PG9, which recognizes high-mannose glycans and protein (38). Complex-type glycan recognition by HIV-1 bNAbs has not been previously documented. Here we describe the properties of bNAbs related to PGT121, some of which, like PGT121, recognize complex-type *N*-glycans in protein-free microarrays.

PGT121 is a glycan-dependent bNAb that was originally identified in the serum of a clade A-infected donor in a functional screen

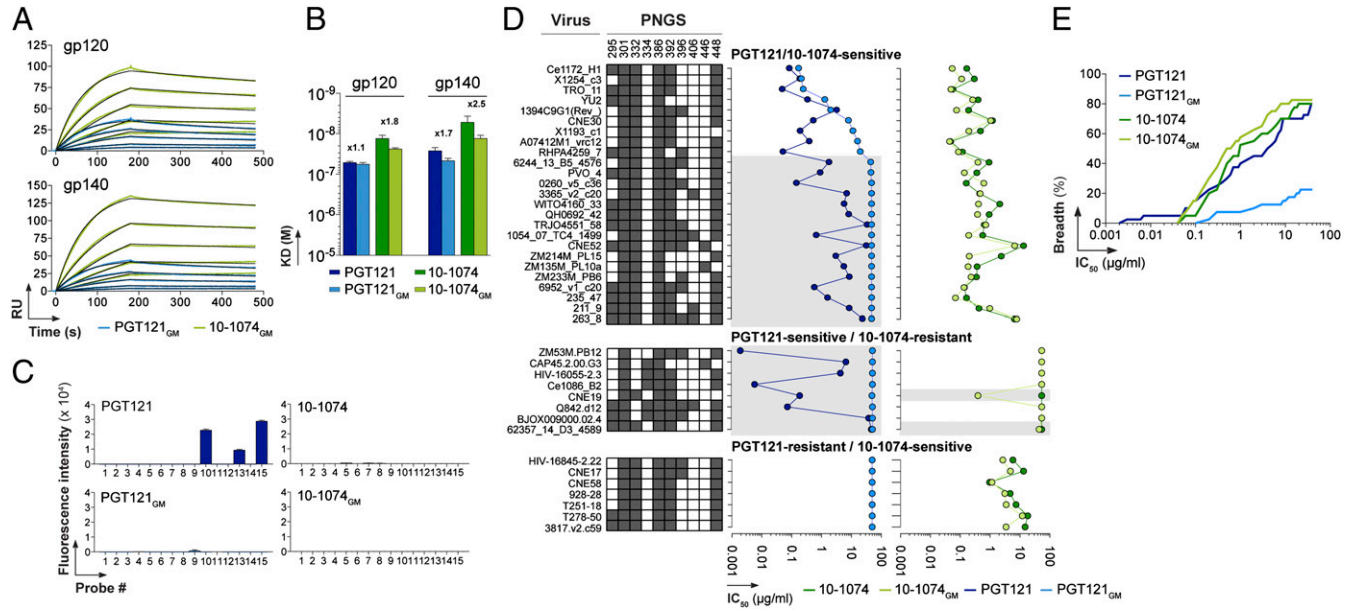

Fig. 5. Binding and neutralization activities of PGT121$_{GM}$ and 10-1074$_{GM}$ mutant antibodies. (*A*) SPR sensorgrams showing the binding of PGT121$_{GM}$ (light green) and 10-1074$_{GM}$ (light blue) to YU-2 gp120 or gp140. (*B*) Bar graphs comparing apparent K_D values for the binding of 10-1074, PGT121, PGT121$_{GM}$, and 10-1074$_{GM}$ antibodies to gp120 and gp140. Error bars indicate the SEM of K_D values obtained from three independent experiments. Fold differences between K_D values of wild-type vs. glycomutant antibodies are indicated. (*C*) Bar graphs comparing binding of glycans (*SI Appendix*, Fig. S6*A*) by PGT121 and 10-1074 with mutant antibodies (PGT121$_{GM}$ and 10-1074$_{GM}$). Numerical scores of binding are measured as fluorescence intensity (means at duplicate spots) for probes arrayed at 5 fmol/spot. (*D*) Graphs comparing IC$_{50}$ values for neutralization of selected viruses by PGT121, 10-1074, PGT121$_{GM}$, and 10-1074$_{GM}$ in the TZM-bl assay. Viral strains are listed with PNGSs at the indicated gp120 positions (those near Asn332$_{gp120}$) color coded: dark gray, a PNGS; white, not a PNGS. From the 2012 Los Alamos filtered web alignment of ~2,865 gp120 sequences, the frequencies of PNGSs at these positions are 295 (58.3%), 301 (91.7%), 332 (73.0%), 334 (20.4%), 386 (86.7%), 392 (79.4%), 396 (25.7%), 406 (5.5%), 446 (7.6%), and 448 (85.6%). Gray shading indicates PGT121-sensitive viruses that were not neutralized by PGT121$_{GM}$ and a 10-1074–resistant strain that was neutralized by 10-1074$_{GM}$. (*E*) Coverage graph comparing the neutralization breadth and potencies of PGT121, PGT121$_{GM}$, 10-1074, and 10–1074$_{GM}$ antibodies in the TZM-bl assay against a panel of 40 viruses.

yielding only two clonally related members (32). We used gp140 trimers as bait for single-cell sorting (44) to isolate 29 new clonal variants of PGT121 (39). The PGT121 clonal family includes distinct groups of closely related antibodies: the PGT121 and 10-1074 groups. Our results suggest that the epitopes of both groups involve the PNGS at $Asn332_{gp120}$ and the base of the V3 loop (*SI Appendix, Discussion*). Serological studies of broad and potent anti–HIV-1 antibodies in humans and SHIV-infected macaques demonstrate that the $Asn332_{gp120}$ PNGS is a frequent target on the HIV spike (6, 55–58). The PGT121-like and 10-1074–like antibody groups differ in amino acid sequences, gp120/gp140 binding affinities, and neutralizing activities, with the 10-1074–like antibodies being completely dependent for neutralization upon an intact PNGS at $Asn332_{gp120}$, whereas PGT121-like antibodies were able to neutralize some viral strains lacking the $Asn332_{gp120}$ PNGS (*SI Appendix, Discussion*). Thus, the immune response in the PGT121 donor developed a mechanism to overcome variations in the HIV glycan shield in part by producing clonal antibody variants with different fine specificities for recognizing an epitope at or near the $Asn332_{gp120}$ PNGS.

A notable difference between the two antibody groups is that the PGT121-like antibodies bound complex-type *N*-glycans in carbohydrate arrays, whereas the 10-1074–like antibodies showed no detectable binding to any of the protein-free *N*-glycans tested (*SI Appendix*, Fig. S6). Protein-free glycan binding by anti-HIV antibodies is not always detectable; e.g., although PG9 recognizes a gp120-associated high-mannose glycan (38), no binding to protein-free glycans was detected in microarrays. Thus, although a positive result in a glycan microarray implies involvement of a particular glycan in an antibody epitope, a negative result does not rule out glycan recognition. For example, although not detectable in the glycan microarray experiments, high-mannose glycans may be involved in the PGT121 epitope, consistent with binding and neutralization of high-mannose-only forms of gp120 protein and virions (*SI Appendix*, Fig. S7).

The molecular basis for the differences between PGT121, 10-1074, and their GL progenitor was revealed in part by their crystal structures. The finding that the majority of light-chain somatic mutations are shared between PGT121 and 10-1074, whereas mutations in the heavy chains differ, suggests that the light-chain contacts shared portions of the gp120 epitope and the heavy chain recognizes distinct features. All three antibodies exhibit an extended CDRH3 with a nonpolar tip that may allow accessing of cryptic epitopes. Differences in the antigen-binding site of the two mature Fabs were mainly localized to a cleft between CDRH2 and the extended CDRH3 (Fig. 3 *C* and *D* and *SI Appendix*, Fig. S14). Interestingly, the putative antigen-binding cleft between CDRH2 and CDRH3 was also found in a representative germ-line progenitor of PGT121 and 10-1074.

We obtained structural information concerning glycan recognition by PGT121-like antibodies from a crystal structure in which a complex-type sialylated *N*-glycan attached to a V_H domain residue interacted with the combining site of a neighboring PGT121 Fab (*SI Appendix*, Fig. S16*A*). Several features of the liganded PGT121 structure suggest it is relevant for understanding the recognition of complex-type *N*-glycans on gp120 by PGT121-like antibodies. First, the glycan in the structure corresponds to the α2–6 sialylated glycan A2(2–6) that PGT121 binds in microarrays (*SI Appendix*, Fig. S6). Second, the glycan interacts with PGT121 using the cleft between CDRH3 and CDRH2 that was suggested by structural analyses to be involved in epitope recognition, potentially explaining the unusual tilting of CDRH3 toward V_L in the PGT121 and 10-1074 structures (Fig. 3 and *SI Appendix*, Fig. S13). Third, most of the V_H residues identified as interacting with the glycan differ between PGT121 and 10-1074 (Fig. 3 *C* and *D*), rationalizing different binding profiles in glycan microarrays and potentially explaining the different fine specificities revealed in protein-binding experiments (Fig. 1). Fourth, swapping crystallographically identified glycan contact residues between PGT121 and 10-1074 in part transferred their properties: $PGT121_{GM}$, like 10-1074, did not bind to protein-free glycans, but both $PGT121_{GM}$ and $10\text{-}1074_{GM}$ preserved near–wild-type binding to purified YU-2 gp120/gp140. Although $PGT121_{GM}$ retained the ability to neutralize some viral strains that were neutralized by wild-type PGT121 and 10-1074, it failed to neutralize strains that are PGT121 sensitive/10-1074 resistant (Fig. 5*D*), demonstrating that the glycan-binding motif is essential for the neutralizing activity of PGT121 against 10-1074–resistant strains. For the reciprocal swap, the neutralization potency of $10\text{-}1074_{GM}$ was increased or unaffected relative to 10-1074, and, in one case, $10\text{-}1074_{GM}$ potently neutralized a PGT121-sensitive/10-1074–resistant strain, consistent with transfer of the crystallographically identified glycan motif and the hypothesis that the epitopes of PGT121-like and 10-1074–like antibodies are related. Taken together, these observations argue that at least part of the glycan epitope recognized by PGT121-like antibodies is revealed by the liganded PGT121 structure.

In the absence of a cocrystal structure of an antibody–gp120 complex, it is difficult to determine the molecular details of the involvement of *N*-glycan in recognition by PGT121-related antibodies. The findings to be reconciled include (*i*) protein-free complex-type *N*-glycan binding by PGT121-like, but not 10-1074–like, antibodies; (*ii*) recognition by both antibody families of high-mannose-only forms of HIV envelopes in solution and on virions; (*iii*) epitope mapping studies reported here and previously for PGT121 (32), implicating the $Asn332_{gp120}$ PNGS; and (*iv*) mutagenesis studies reported here and previously for PGT121 (32) that failed to find a second PNGS affecting binding or neutralization.

One interpretation of these findings is that PGT121-like antibodies exhibit promiscuous carbohydrate recognition properties such that they could accommodate either a complex-type or a high-mannose *N*-glycan attached to $Asn332_{gp120}$. However, this PNGS is generally assumed to carry high-mannose *N*-glycans on the basis of mass spectrometry data (50, 59–67) and the fact that it forms a critical part of the epitope recognized by the high-mannose–specific antibody 2G12 (46, 47). Nonetheless, the possibility of complex-type glycan at this position under some circumstances remains open given that the $Asn332_{gp120}$-linked *N*-glycan has been reported to be a mixture of high mannose and complex type in gp140s from some viral strains (42). In general, definitive assignment of glycan composition on HIV-1 envelope spikes is complicated by studies showing that the composition of *N*-linked glycans is heterogeneous within a single viral strain or purified envelope construct and can differ at individual PNGSs on the basis of the viral strain and whether the glycans were analyzed on virions or purified proteins. In the case of virions, glycan composition can depend on whether virions were produced as pseudoviruses or from a single-plasmid production system, and, in the case of purified proteins, glycan composition can differ depending on the oligomeric state of the purified envelope being examined (monomeric gp120 vs. trimeric gp140) and the cell type used for expression (42, 50, 59–63, 65). Indeed, marked cell-to-cell differences are known to occur in carbohydrate sequences within established cell lines (68).

A second interpretation of the available data is that PGT121-like antibodies have binding sites that can accommodate a high-mannose glycan attached to $Asn332_{gp120}$ and either a complex-type or a high-mannose *N*-glycan attached to a second, as yet unidentified, PNGS that was not detected in our mutagenesis experiments (*SI Appendix*, Fig. S5) or those previously conducted for PGT121 (32). Unfortunately, there is no direct way to assess the nature of the glycan(s) recognized at the $Asn332_{gp120}$ PNGS and/or a putative second PNGS because it is not possible to selectively convert one or all PNGSs to exclusively complex-type glycans on virions or recombinant proteins. Thus, although we were able to demonstrate binding to and neutralization of high-mannose-only proteins and virions by PGT121-like and 10-1074–like antibodies, we cannot perform the reciprocal experiment to assess binding and neutralization of complex-type-only proteins and virions. Nonetheless, adding the discovery that PGT121 can bind complex-type *N*-glycans to the literature describing high-mannose *N*-glycan recognition by HIV antibodies (32, 33, 37, 38,

46, 47) suggests that the host immune system can respond to both high-mannose and complex-type glycans on gp120.

Given that any changes in the Asn332$_{gp120}$ PNGS (substitutions at either position 332 or 334) affect neutralization by 10-1074–like antibodies (*SI Appendix*, Table S5), their epitopes likely also include Asn332$_{gp120}$-attached glycan or, alternatively, a glycan-modulated conformational protein epitope. As 10-1074–like antibodies showed no detectable binding to any protein-free glycans (*SI Appendix*, Fig. S6), we have no information about the nature of their putatively recognized glycan(s). However, our data suggest the possibility that 10-1074–like and PGT121-like antibodies have different glycan preferences, with 10-1074–like antibodies preferring high-mannose *N*-glycans to complex type, and PGT121-like antibodies exhibiting the opposite preference. This speculation is consistent with Endo H treatment of gp120 that contained both complex-type and high-mannose *N*-glycans, resulting in a greater decrease in binding of 10-1074–like than PGT121-like antibodies (Fig. 1*E*) and gp120$_{kif}$ showing decreased binding to PGT121-like antibodies, but equivalent binding to 10-1074–like antibodies. In addition, the concentration of sequence differences between PGT121 and 10-1074 in the glycan-binding site of PGT121 (Figs. 3 and 4) suggests structurally distinct features of their related epitopes, which could be accessed by slightly different angles of approach to binding of gp120 within an envelope spike.

Although further studies will be required to define the details, our results raise the possibility that recognition of gp120 glycans by HIV antibodies such as PGT121 can involve both high-mannose and complex-type *N*-glycans in a carbohydrate-dependent epitope. Other carbohydrate-dependent HIV antibodies, such as PGT128, may share this property. This would be an advantageous adaptation of the host immune system to deal with heterogeneous *N*-glycan compositions on HIV-1 envelope spikes. The PGT128/gp120 outer domain–V3 crystal structure reveals a mechanism by which promiscuous recognition of either complex-type or high-mannose *N*-glycan at a particular PNGS might be accomplished in that contacts between PGT128 and the Asn301$_{gp120}$-linked high-mannose glycan involve only the core pentasaccharide (37), a portion that is common to both high-mannose and complex-type *N*-glycans. This raises the possibility that PGT128 binding would not be abrogated by a complex-type *N*-glycan attached to Asn301$_{gp120}$; indeed the Asn301$_{gp120}$-attached carbohydrate appears to be a complex-type *N*-glycan in gp120s that were analyzed by mass spectrometry (50, 60, 66) but not in the gp120 outer domain construct used for the structural studies, which was produced in GnTI $^{-/-}$ cells (37). By analogy, although PGT121-like antibodies may prefer interactions with a complex-type *N*-glycan, as suggested by our glycan microarray results (Fig. 1*E* and *SI Appendix*, Fig. S6) and the liganded PGT121 structure (Fig. 4), these antibodies may be able to accommodate either a complex-type or a high-mannose glycan at a PNGS through interactions with the core pentasaccharide, possibly combined with contacts to the asparagine or nearby protein residues.

Promiscuity in glycan recognition suggests a mechanism to explain why PGT121-like and 10-1074–like antibodies, like PGT128 (37), exhibit saturable curves in neutralization assays (*SI Appendix*, Fig. S10*C*), in contrast to PG9 and PG16 neutralization curves, which plateau at values less than 100% (33): Assuming that PGT121, PGT128, and 10-1074 are more promiscuous with respect to *N*-glycan recognition than PG9/PG16, then although the former antibodies might prefer either complex-type (PGT121) or high-mannose (PGT128) glycans, they could still bind to those spikes and/or virions within a given strain that carry the less desirable glycan at a particular *N*-linked site (perhaps by interacting with only the pentasaccharide core). In contrast, PG9/PG16 may have an absolute requirement for high-mannose *N*-glycans and therefore would be unable to neutralize all virions in a heterogeneous mixture of viruses with different glycan compositions, thereby rationalizing the shallow neutralization curves that plateau at less than 100% neutralization (33).

Promiscuity with respect to carbohydrate interactions would be an advantageous adaptation for an HIV antibody as a mechanism ensuring neutralization of all viruses within a given strain. This suggests that immunogens should be designed and produced such that they can contain complex-type *N*-glycans to elicit antibodies that can recognize these structures. Previous studies of carbohydrate-dependent HIV antibodies characterized interactions with high-mannose *N*-glycans; our functional and structural studies of PGT121-like antibodies now provide information regarding HIV antibodies that likely recognize complex-type, as well as high-mannose, *N*-glycans in their epitopes on gp120. PGT121 is a member of a large group of neutralizing antibodies that recognize the V3 region of HIV (30, 39, 69–71), which has variable amino acid sequence and carbohydrate composition in different HIV isolates (71). Nevertheless, there is sufficient conservation that antibodies against the V3 region can be broadly neutralizing by targeting the V3 crown (71) or carbohydrates and the base of the V3 loop (PGT121 and PGT128). The diversity of glycan and peptide recognition by the combination of PGT121, 10-1074, and PGT128 appears to disarm the HIV glycan shield. Thus, vaccines designed to elicit antibodies to this region would likely be most effective by including epitopes recognized by all types of V3 antibodies.

Materials and Methods

Single B-Cell RT-PCRs and Ig Gene Analyses. Single-cell sorting of gp140^{+}CD19^{+}IgG^{+} B cells from patient 10 (pt10) (referred to as patient 17 in ref. 32) PBMCs, cDNA synthesis, and nested PCR amplifications of Ig genes were performed in a previous study (39). Igλ genes expressed by PGT121 clonal variants were PCR amplified using a forward primer (L-Vλ3–21*02: 5′ CTGGACCGTTCTCCTCCTCG 3′) farther upstream in the leader region to avoid the potentially mutated region (31). All PCR products were sequenced and analyzed for Ig gene use, CDR3 analyses, and number of VH/Vκ somatic hypermutations (IgBLAST, www.ncbi.nlm.nih.gov/igblast; and IMGT, www.imgt.org). Multiple sequence alignments were performed using the MacVector program (v.12.5.0) with the ClustalW analysis function (default parameters) and were used to generate dendrograms by the neighbor-joining method (with Best tree mode and outgroup rooting). Alternatively, dendrograms shown in Figs. 1*E*, 2*A*, and 4*D* were generated using the UPGMA method (with Best tree mode).

Cloning and Production of Antibodies. Purified digested PCR products were cloned into human Igγ$_1$-, or Igλ-expressing vectors as previously described (40). Vectors containing IgH and Igλ genes were then sequenced and compared with the original PCR product sequences. PGT121 and 10-303 shared the same Igλ gene and had 1 aa difference in position 2 of the IgH gene (*SI Appendix*, Fig. S2); therefore to produce the PGT121 IgG, we used the 10-303 Igλ gene and a PGT121 IgH gene generated by introducing a single substitution (V2M) into the 10-303 IgH gene by site-directed mutagenesis (QuikChange Site-Directed Mutagenesis Kit; Stratagene). To generate His-tagged Fabs, the PGT121 and 10-1074 V_H genes were subcloned into a 6xHis-IgCγ1 expression vector generated by modifying our standard Igγ$_1$ vector (41) to encode the IgG1 C_H1 domain followed by a 6x-His tag. IgH DNA fragments encoding PGT121$_{GM}$ (S32Y, K53D, S54R, N58T, H97R, and T100lY) and 10-1074$_{GM}$ (Y32S, D53K, R54S, T58N, R97H, and Y100lT) mutant antibodies were obtained as a synthetic minigene (IDT) and subcloned into Igγ$_1$-expressing vectors. Antibodies and Fab fragments were produced by transient transfection of IgH and IgL expression plasmids into exponentially growing HEK 293T cells (ATCC; CRL-11268), using the polyethyleneimine (PEI)-precipitation method (39). IgG antibodies were affinity purified using Protein G Sepharose beads (GE Healthcare) according to the manufacturer's instructions. Fab fragments were affinity purified using HisPur Cobalt Resin (Thermo Scientific) as described below.

HIV-1 Env Proteins. Alanine mutations were introduced into the pYU-2 gp120 vector (gift of J. Sodroski, Harvard Medical School) at positions 301–303 (Asn-Asn-Thr), 324–325 (Gly-Asp), and 332 (Asn) (HXBc2 amino acid numbering), using the QuikChange Site-Directed Mutagenesis kit (Stratagene) according to the manufacturer's instructions. The same procedure was used to generate "double-glycan" mutants by introducing single alanine mutations in the pYU-2 gp120^{N332A} vector at each PNGS located between Asn262$_{gp120}$ and Asn406$_{gp120}$. Site-directed mutations were verified by DNA sequencing. Expression vectors encoding YU-2 gp140 (72), YU-2 gp120, HXB2c gp120^{core} (73), and HXB2c 2CCcore (74) proteins and YU-2 gp120 mutant proteins were used to transfect HEK 293T cells as previously described (39). To produce

high-mannose-only YU-2 gp120 protein ($gp120_{kif}$), 25 μM kifunensine (Enzo Life Sciences) was added at the time of transfection. Culture supernatants were harvested and concentrated using centrifugation-based filtration devices (Vivacell 100; Sartorius Stedim Biotech) that allowed buffer exchange of the samples into 10 mM imidazole, 50 mM sodium phosphate, 300 mM sodium chloride, pH 7.4. Proteins were purified by affinity chromatography, using HisPur Cobalt Resin (Thermo Scientific) according to the manufacturer's instructions. For deglycosylation reactions, 50 μg of HEK 293T cell-produced YU-2 gp120 in PBS was digested overnight at 37 °C with 200 units of PNGase F (New England Biolabs) or 10,000 units of Endo H_f (New England Biolabs) in their respective reaction buffers without denaturing agents. After buffer exchange into PBS using Centrifugal Filters (Amicon Ultra, Millipore), glycosidase-treated gp120s (200 ng) were examined by SDS/PAGE, using a 4–12% NuPAGE gel (Invitrogen) followed by silver staining (Pierce Silver Stain Kit; Thermo Scientific).

ELISAs. High-binding 96-well ELISA plates (Costar) were coated overnight with 100 ng/well of purified gp120 in PBS. After washing, the plates were blocked for 2 h with 2% (wt/vol) BSA, 1 μM EDTA, and 0.05% Tween-PBS (blocking buffer) and then incubated for 2 h with IgGs at concentrations of 26.7 nM (or 427.2 nM for ELISAs using the YU-2 gp120 double-glycan mutants) and seven consecutive 1:4 dilutions in PBS. After washing, the plates were developed by incubation with goat HRP-conjugated anti-human IgG antibodies (Jackson ImmunoReseach) (at 0.8 μg/mL in blocking buffer) for 1 h and by addition of HRP chromogenic substrate (ABTS solution; Invitrogen) as previously described (39). Antibody binding to the selected $gp120^{V3}$ overlapping peptides was tested using a previously described peptide-ELISA method (39). For competition ELISAs, gp120-coated plates were blocked for 2 h with blocking buffer and then incubated for 2 h with biotinylated antibodies (at a concentration of 26.6 nM for PGT121, 0.21 nM for 10-1074, 0.43 nM for 10-996, and 1.67 nM for 10-1369) in 1:2 serially diluted solutions of antibody competitors in PBS (IgG concentration range from 5.2 to 667 nM). Plates were developed as described above, using HRP-conjugated streptavidin (Jackson ImmunoReseach) (at 0.8 μg/mL in blocking buffer). All experiments were performed at least in duplicate.

Glycan Microarray Analysis. Microarrays were generated by robotically printing glycan probes linked to lipid (neoglycolipids) onto nitrocellulose-coated glass slides as described in refs. 75 and 76 at two levels (2 and 5 fmol/spot) in duplicate. Binding assays were performed with microarrays containing 15 neoglycolipids derived from *N*-glycans of high-mannose and complex types. The sequences of the probes are shown in *SI Appendix*, Fig. S6*A*. In brief, antibodies were tested at 50 μg/mL, and binding was detected with biotinylated anti-human IgG (Vector) followed by AlexaFluor 647-labeled streptavidin (Molecular Probes).

Surface Plasmon Resonance. Experiments were performed using a Biacore T100 as described previously (77). Briefly, YU-2 gp140 and gp120 proteins were primary-amine coupled on CM5 chips (Biacore) at a coupling density of 300 response units (RU). Anti-gp120 IgGs and the GL precursor were injected over flow cells at 1 μM and 10 μM, respectively, at flow rates of 35 μL/min with 3-min association and 5-min dissociation phases. The sensor surface was regenerated by a 30-s injection of 10 mM glycine·HCl, pH 2.5, at a flow rate of 50 μL/min. Dissociation [k_d (s^{-1})], association [k_a ($M^{-1}{\cdot}s^{-1}$)], and binding constants [K_D (M) or K_A (M^{-1})] were calculated from kinetic analyses after subtraction of backgrounds using a 1:1 binding model without a bulk reflective index (RI) correction (Biacore T100 Evaluation software). Binding constants for bivalent IgGs calculated using a 1:1 binding model are referred to in the text as "apparent" affinities to emphasize that the K_D values include potential avidity effects.

Neutralization Assays. Virus neutralization was evaluated using a luciferase-based assay in TZM.bl cells as previously described (49). The HIV-1 pseudoviruses tested contained mostly tier-2 and tier-3 viruses (78) (*SI Appendix*, Tables S2 and S3). High-mannose-only pseudoviruses were produced in wild-type cells treated with 25 μM kifunensine (Enzo Life Sciences) (*SI Appendix*, Fig. S7*C*) or in HEK 293S GnTI$^{-/-}$ cells (*SI Appendix*, Fig. S7*D*). Nonlinear regression analysis was used to calculate concentrations at which half-maximal inhibition was observed (IC_{50} values). Neutralization activities were also evaluated with a previously characterized PBMC-based assay, using infection with primary HIV-1 variants (n = 95) isolated from clade B-infected donors with known seroconversion dates either between 1985 and 1989 ("historical seroconverters," n = 14) or between 2003 and 2006 ("contemporary seroconverters," n = 21) (51, 52). Neutralization activity for each antibody was calculated using GraphPad Prism software (v5.0b) as area under the best-fit curve, which fits the proportion of viruses neutralized over IC_{50} values ranging from 0.001 to 50 μg/mL. Relative area under the curve (RAUC) values were derived by normalizing all AUC values by the highest value (obtained with 10-1074).

Statistical Analyses. Statistical analyses were performed with the GraphPad Prism software (v5.0b). Neutralization potencies in the TZM-bl assay against the selected panel of nine virus strains vs. the apparent binding affinities of the antibodies for gp120 and gp140 were analyzed using Spearman's correlation test. The Mann–Whitney test was used to compare (*i*) affinities for gp120/gp140 of antibodies belonging to the PGT121 or 10-1074 group and (*ii*) neutralization activities against viruses isolated from historical and contemporary seroconverters.

Crystallization and Structure Determinations. Crystallization, data collection, structure determinations, and analyses are described in detail in *SI Appendix*. The atomic models were refined to 3.0-Å resolution for PGT121 Fab (R_{work} = 21.6%; R_{free} = 26.4%), 1.9-Å resolution for 10-1074 Fab (R_{work} = 18.7%; R_{free} = 22.3%), 2.4-Å resolution for four GL Fab molecules (R_{work} = 19.4%; R_{free} = 23.7%), and 2.4-Å resolution for liganded PGT121 Fab (R_{work} = 20.1%; R_{free} = 24.9%). The atomic model of PGT121 Fab contains 95.2%, 4.9%, and 0.0% of the residues in the favored, allowed, and disallowed regions of the Ramachandran plot, respectively (10-1074 Fab, 98.8%, 0.9%, and 0.2%; GL Fab, 96.0%, 3.8%, and 0.23%; and liganded PGT121 Fab, 96.7%, 3.1%, and 0.2%).

ACKNOWLEDGMENTS. We thank Tim Feliciano and the Caltech Protein Expression Center for expression of proteins, Terri Lee for producing pseudoviruses in HEK 293S GnTI $^{-/-}$ cells, Anthony West for germ-line gene analyses, and the T.F. laboratory for establishing the neoglycolipid-based microarray system. This research was supported by The Rockefeller University, National Institutes of Health Grant 1 P01 AI081677 (to M.C.N.), the International AIDS Vaccine Initiative and the Bill and Melinda Gates Foundation [Comprehensive Antibody-Vaccine Immune Monitoring Consortium Grant 1032144 (to M.S.S.); Collaboration for AIDS Vaccine Discovery Grants 38660 (to P.J.B.) and 38619s (to M.C.N.)], UK Research Councils' Basic Technology Initiative "Glycoarrays" Grant GRS/79268, Engineering and Physical Sciences Research Council Translational Grant EP/G037604/1, Wellcome Trust Grant WT093378MA, National Cancer Institute Alliance of Glycobiologists for Detection of Cancer and Cancer Risk Grant U01 CA128416, and the Molecular Observatory at Caltech supported by the Gordon and Betty Moore Foundation. Operations at the Stanford Synchrotron Radiation Lightsource are supported by the US Department of Energy and the National Institutes of Health. M.C.N. and P.J.B. are Howard Hughes Medical Institute investigators.

1. Plotkin SA (2008) Vaccines: Correlates of vaccine-induced immunity. *Clin Infect Dis* 47 (3):401–409.
2. Haynes BF, et al. (2012) Immune-correlates analysis of an HIV-1 vaccine efficacy trial. *N Engl J Med* 366(14):1275–1286.
3. Simek MD, et al. (2009) Human immunodeficiency virus type 1 elite neutralizers: Individuals with broad and potent neutralizing activity identified by using a high-throughput neutralization assay together with an analytical selection algorithm. *J Virol* 83(14):7337–7348.
4. Sather DN, et al. (2009) Factors associated with the development of cross-reactive neutralizing antibodies during human immunodeficiency virus type 1 infection. *J Virol* 83(2):757–769.
5. Gray ES, et al. (2009) Antibody specificities associated with neutralization breadth in plasma from human immunodeficiency virus type 1 subtype C-infected blood donors. *J Virol* 83(17):8925–8937.
6. Gray ES, et al.; and the CAPRISA002 Study Team (2011) The neutralization breadth of HIV-1 develops incrementally over four years and is associated with CD4+ T cell decline and high viral load during acute infection. *J Virol* 85(10):4828–4840.
7. Doria-Rose NA, et al. (2009) Frequency and phenotype of human immunodeficiency virus envelope-specific B cells from patients with broadly cross-neutralizing antibodies. *J Virol* 83(1):188–199.
8. Dhillon AK, et al. (2007) Dissecting the neutralizing antibody specificities of broadly neutralizing sera from human immunodeficiency virus type 1-infected donors. *J Virol* 81(12):6548–6562.
9. Binley JM, et al. (2008) Profiling the specificity of neutralizing antibodies in a large panel of plasmas from patients chronically infected with human immunodeficiency virus type 1 subtypes B and C. *J Virol* 82(23):11651–11668.
10. Mascola JR, Montefiori DC (2010) The role of antibodies in HIV vaccines. *Annu Rev Immunol* 28:413–444.
11. Bunnik EM, Pisas L, van Nuenen AC, Schuitemaker H (2008) Autologous neutralizing humoral immunity and evolution of the viral envelope in the course of subtype B human immunodeficiency virus type 1 infection. *J Virol* 82(16):7932–7941.
12. Richman DD, Wrin T, Little SJ, Petropoulos CJ (2003) Rapid evolution of the neutralizing antibody response to HIV type 1 infection. *Proc Natl Acad Sci USA* 100(7): 4144–4149.

13. Wei X, et al. (2003) Antibody neutralization and escape by HIV-1. *Nature* 422(6929): 307–312.
14. Baba TW, et al. (2000) Human neutralizing monoclonal antibodies of the IgG1 subtype protect against mucosal simian-human immunodeficiency virus infection. *Nat Med* 6(2):200–206.
15. Hessell AJ, et al. (2009) Effective, low-titer antibody protection against low-dose repeated mucosal SHIV challenge in macaques. *Nat Med* 15(8):951–954.
16. Hessell AJ, et al. (2009) Broadly neutralizing human anti-HIV antibody 2G12 is effective in protection against mucosal SHIV challenge even at low serum neutralizing titers. *PLoS Pathog* 5(5):e1000433.
17. Hessell AJ, et al. (2010) Broadly neutralizing monoclonal antibodies 2F5 and 4E10 directed against the human immunodeficiency virus type 1 gp41 membrane-proximal external region protect against mucosal challenge by simian-human immunodeficiency virus SHIVBa-L. *J Virol* 84(3):1302–1313.
18. Mascola JR, et al. (1999) Protection of Macaques against pathogenic simian/human immunodeficiency virus 89.6PD by passive transfer of neutralizing antibodies. *J Virol* 73(5):4009–4018.
19. Mascola JR, et al. (2000) Protection of macaques against vaginal transmission of a pathogenic HIV-1/SIV chimeric virus by passive infusion of neutralizing antibodies. *Nat Med* 6(2):207–210.
20. Ng CT, et al. (2010) Passive neutralizing antibody controls SHIV viremia and enhances B cell responses in infant macaques. *Nat Med* 16(10):1117–1119.
21. Parren PW, et al. (2001) Antibody protects macaques against vaginal challenge with a pathogenic R5 simian/human immunodeficiency virus at serum levels giving complete neutralization in vitro. *J Virol* 75(17):8340–8347.
22. Shibata R, et al. (1999) Neutralizing antibody directed against the HIV-1 envelope glycoprotein can completely block HIV-1/SIV chimeric virus infections of macaque monkeys. *Nat Med* 5(2):204–210.
23. Trkola A, et al. (2005) Delay of HIV-1 rebound after cessation of antiretroviral therapy through passive transfer of human neutralizing antibodies. *Nat Med* 11(6):615–622.
24. Veazey RS, et al. (2003) Prevention of virus transmission to macaque monkeys by a vaginally applied monoclonal antibody to HIV-1 gp120. *Nat Med* 9(3):343–346.
25. Karlsson Hedestam GB, et al. (2008) The challenges of eliciting neutralizing antibodies to HIV-1 and to influenza virus. *Nat Rev Microbiol* 6(2):143–155.
26. Mascola JR (2007) HIV/AIDS: Allied responses. *Nature* 449(7158):29–30.
27. Montefiori DC, Mascola JR (2009) Neutralizing antibodies against HIV-1: Can we elicit them with vaccines and how much do we need? *Curr Opin HIV AIDS* 4(5):347–351.
28. Zolla-Pazner S (2004) Identifying epitopes of HIV-1 that induce protective antibodies. *Nat Rev Immunol* 4(3):199–210.
29. Bonsignori M, et al. (2011) Analysis of a clonal lineage of HIV-1 envelope V2/V3 conformational epitope-specific broadly neutralizing antibodies and their inferred unmutated common ancestors. *J Virol* 85(19):9998–10009.
30. Corti D, et al. (2010) Analysis of memory B cell responses and isolation of novel monoclonal antibodies with neutralizing breadth from HIV-1-infected individuals. *PLoS ONE* 5(1):e8805.
31. Scheid JF, et al. (2011) Sequence and structural convergence of broad and potent HIV antibodies that mimic CD4 binding. *Science* 333(6049):1633–1637.
32. Walker LM, et al.; Protocol G Principal Investigators (2011) Broad neutralization coverage of HIV by multiple highly potent antibodies. *Nature* 477(7365):466–470.
33. Walker LM, et al. (2009) Broad and potent neutralizing antibodies from an African donor reveal a new HIV-1 vaccine target. *Science* 326(5950):285–289.
34. Wu X, et al. (2010) Rational design of envelope identifies broadly neutralizing human monoclonal antibodies to HIV-1. *Science* 329(5993):856–861.
35. Wu X, et al.; NISC Comparative Sequencing Program (2011) Focused evolution of HIV-1 neutralizing antibodies revealed by structures and deep sequencing. *Science* 333 (6049):1593–1602.
36. Diskin R, et al. (2011) Increasing the potency and breadth of an HIV antibody by using structure-based rational design. *Science* 334(6060):1289–1293.
37. Pejchal R, et al. (2011) A potent and broad neutralizing antibody recognizes and penetrates the HIV glycan shield. *Science* 334(6059):1097–1103.
38. McLellan JS, et al. (2011) Structure of HIV-1 gp120 V1/V2 domain with broadly neutralizing antibody PG9. *Nature* 480(7377):336–343.
39. Mouquet H, et al. (2011) Memory B cell antibodies to HIV-1 gp140 cloned from individuals infected with clade A and B viruses. *PLoS ONE* 6(9):e24078.
40. Tiller T, et al. (2008) Efficient generation of monoclonal antibodies from single human B cells by single cell RT-PCR and expression vector cloning. *J Immunol Methods* 329(1–2):112–124.
41. Wardemann H, et al. (2003) Predominant autoantibody production by early human B cell precursors. *Science* 301(5638):1374–1377.
42. Go EP, et al. (2008) Glycosylation site-specific analysis of HIV envelope proteins (JR-FL and CON-S) reveals major differences in glycosylation site occupancy, glycoform profiles, and antigenic epitopes' accessibility. *J Proteome Res* 7(4):1660–1674.
43. Elbein AD, Tropea JE, Mitchell M, Kaushal GP (1990) Kifunensine, a potent inhibitor of the glycoprotein processing mannosidase I. *J Biol Chem* 265(26):15599–15605.
44. Scheid JF, et al. (2009) Broad diversity of neutralizing antibodies isolated from memory B cells in HIV-infected individuals. *Nature* 458(7238):636–640.
45. Sanders RW, et al. (2002) The mannose-dependent epitope for neutralizing antibody 2G12 on human immunodeficiency virus type 1 glycoprotein gp120. *J Virol* 76(14): 7293–7305.
46. Scanlan CN, et al. (2002) The broadly neutralizing anti-human immunodeficiency virus type 1 antibody 2G12 recognizes a cluster of alpha1—>2 mannose residues on the outer face of gp120. *J Virol* 76(14):7306–7321.
47. Calarese DA, et al. (2003) Antibody domain exchange is an immunological solution to carbohydrate cluster recognition. *Science* 300(5628):2065–2071.
48. Calarese DA, et al. (2005) Dissection of the carbohydrate specificity of the broadly neutralizing anti-HIV-1 antibody 2G12. *Proc Natl Acad Sci USA* 102(38):13372–13377.
49. Li M, et al. (2005) Human immunodeficiency virus type 1 env clones from acute and early subtype B infections for standardized assessments of vaccine-elicited neutralizing antibodies. *J Virol* 79(16):10108–10125.
50. Binley JM, et al. (2010) Role of complex carbohydrates in human immunodeficiency virus type 1 infection and resistance to antibody neutralization. *J Virol* 84(11): 5637–5655.
51. Euler Z, et al. (2011) Activity of broadly neutralizing antibodies, including PG9, PG16, and VRC01, against recently transmitted subtype B HIV-1 variants from early and late in the epidemic. *J Virol* 85(14):7236–7245.
52. Bunnik EM, et al. (2010) Adaptation of HIV-1 envelope gp120 to humoral immunity at a population level. *Nat Med* 16(9):995–997.
53. Zhou T, et al. (2010) Structural basis for broad and potent neutralization of HIV-1 by antibody VRC01. *Science* 329(5993):811–817.
54. Walters RW, et al. (2001) Binding of adeno-associated virus type 5 to 2,3-linked sialic acid is required for gene transfer. *J Biol Chem* 276(23):20610–20616.
55. Tomaras GD, et al. (2011) Polyclonal B cell responses to conserved neutralization epitopes in a subset of HIV-1-infected individuals. *J Virol* 85(21):11502–11519.
56. Walker LM, et al. (2010) A limited number of antibody specificities mediate broad and potent serum neutralization in selected HIV-1 infected individuals. *PLoS Pathog* 6(8): e1001028.
57. Lavine CL, et al.; NIAID Center for HIV/AIDS Vaccine Immunology (CHAVI) (2012) High-mannose glycan-dependent epitopes are frequently targeted in broad neutralizing antibody responses during human immunodeficiency virus type 1 infection. *J Virol* 86 (4):2153–2164.
58. Walker LM, et al. (2011) Rapid development of glycan-specific, broad, and potent anti-HIV-1 gp120 neutralizing antibodies in an R5 SIV/HIV chimeric virus infected macaque. *Proc Natl Acad Sci USA* 108(50):20125–20129.
59. Bonomelli C, et al. (2011) The glycan shield of HIV is predominantly oligomannose independently of production system or viral clade. *PLoS ONE* 6(8):e23521.
60. Cutalo JM, Deterding LJ, Tomer KB (2004) Characterization of glycopeptides from HIV-I(SF2) gp120 by liquid chromatography mass spectrometry. *J Am Soc Mass Spectrom* 15(11):1545–1555.
61. Doores KJ, et al. (2010) Envelope glycans of immunodeficiency virions are almost entirely oligomannose antigens. *Proc Natl Acad Sci USA* 107(31):13800–13805.
62. Go EP, et al. (2009) Glycosylation site-specific analysis of clade C HIV-1 envelope proteins. *J Proteome Res* 8(9):4231–4242.
63. Go EP, et al. (2011) Characterization of glycosylation profiles of HIV-1 transmitted/ founder envelopes by mass spectrometry. *J Virol* 85(16):8270–8284.
64. Leonard CK, et al. (1990) Assignment of intrachain disulfide bonds and characterization of potential glycosylation sites of the type 1 recombinant human immunodeficiency virus envelope glycoprotein (gp120) expressed in Chinese hamster ovary cells. *J Biol Chem* 265(18):10373–10382.
65. Wang L, et al. (2010) Structural analysis of a highly glycosylated and unliganded gp120-based antigen using mass spectrometry. *Biochemistry* 49(42):9032–9045.
66. Zhu X, Borchers C, Bienstock RJ, Tomer KB (2000) Mass spectrometric characterization of the glycosylation pattern of HIV-gp120 expressed in CHO cells. *Biochemistry* 39(37): 11194–11204.
67. Pabst M, Chang M, Stadlmann J, Altmann F (2012) Glycan profiles of the 27 N-glycosylation sites of the HIV envelope protein CN54gp140. *Biol Chem* 393(8): 719–730.
68. Childs RA, Kapadia A, Feizi T (1980) Expression of blood group I and i active carbohydrate sequences on cultured human and animal cell lines assessed by radioimmunoassays with monoclonal cold agglutinins. *Eur J Immunol* 10(5):379–384.
69. Gorny MK, et al. (2002) Human monoclonal antibodies specific for conformation-sensitive epitopes of V3 neutralize human immunodeficiency virus type 1 primary isolates from various clades. *J Virol* 76(18):9035–9045.
70. Hioe CE, et al. (2010) Anti-V3 monoclonal antibodies display broad neutralizing activities against multiple HIV-1 subtypes. *PLoS ONE* 5(4):e10254.
71. Zolla-Pazner S, Cardozo T (2010) Structure-function relationships of HIV-1 envelope sequence-variable regions refocus vaccine design. *Nat Rev Immunol* 10(7):527–535.
72. Yang X, Farzan M, Wyatt R, Sodroski J (2000) Characterization of stable, soluble trimers containing complete ectodomains of human immunodeficiency virus type 1 envelope glycoproteins. *J Virol* 74(12):5716–5725.
73. Kwong PD, et al. (1998) Structure of an HIV gp120 envelope glycoprotein in complex with the CD4 receptor and a neutralizing human antibody. *Nature* 393(6686): 648–659.
74. Dey B, et al. (2009) Structure-based stabilization of HIV-1 gp120 enhances humoral immune responses to the induced co-receptor binding site. *PLoS Pathog* 5(5): e1000445.
75. Liu Y, et al. (2012) Neoglycolipid-based oligosaccharide microarray system: Preparation of NGLs and their noncovalent immobilization on nitrocellulose-coated glass slides for microarray analyses. *Methods Mol Biol* 808:117–136.
76. Palma AS, et al. (2006) Ligands for the beta-glucan receptor, Dectin-1, assigned using "designer" microarrays of oligosaccharide probes (neoglycolipids) generated from glucan polysaccharides. *J Biol Chem* 281(9):5771–5779.
77. Mouquet H, et al. (2010) Polyreactivity increases the apparent affinity of anti-HIV antibodies by heteroligation. *Nature* 467(7315):591–595.
78. Seaman MS, et al. (2010) Tiered categorization of a diverse panel of HIV-1 Env pseudoviruses for assessment of neutralizing antibodies. *J Virol* 84(3):1439–1452.